

## OPDISM

### Optical Parameters Determined by Integrating Sphere Measurement

**Xin-Hua Hu, Cheng Chen, Jun Q. Lu**

[Biomedical Laser Laboratory](#), Department of Physics, East Carolina University  
Greenville, North Carolina 27858, USA

#### *Abstract*

This is a manual written collectively by the above authors in the [Biomedical Laser Laboratory](#) to describe a method for determination of optical parameters of turbid samples. The measured signals are acquired with spatial filtering and integrating sphere and calculated signals are obtained with an individual Monte Carlo (iMC) simulation code. We provided in this manual the description of the Monte Carlo simulation code for photon transportation in a turbid sample of slab form and the related gradient based inverse algorithm.

#### *Acknowledgement*

The method described in this manual has been developed by the above authors and other researchers in the Biomedical Laser Laboratory since 1999 (Song, 1999; Lu, 2000; Du, 2001; Ma, 2003; Ma, 2003; Ma, 2005). We would like to acknowledge the Monte Carlo code (MCML) developed by Lihong Wang et al. (Wang, 1995) whose structural design has been utilized to improve the code structure of our early versions. We would like to thank Zhi Song and Ke Dong for their contributions to the early versions of our Monte Carlo code; Yong Du, Kenneth Jacobs and Xiaoyan Ma for their contributions to the signal measurements described in this manual.

## Table of Contents

<b>Chapter 1</b>	<b>Inverse problems and radiative transfer .....</b>	<b>4</b>
§1.1	The inverse problem .....	4
§1.2	The tools .....	5
<b>Chapter 2</b>	<b>Signal measurement .....</b>	<b>6</b>
§2.1	Measurement of light signals of collimated transmission .....	6
§2.2	Measurement of diffuse reflectance and transmittance .....	6
<b>Chapter 3</b>	<b>The Monte Carlo code.....</b>	<b>8</b>
§3.1	Essence of Monte Carlo (MC) simulation.....	8
§3.2	Details of iMC code .....	9
§3.2.1	monte_define.....	11
§3.2.2	monte_io .....	11
§3.2.3	monte_sub .....	11
§3.2.4	monte_go.....	11
§3.2.5	monte_main.....	12
§3.3	How to run the iMC code? .....	13
§3.4	Code validation .....	13
<b>References .....</b>		<b>14</b>

**Acronyms and Symbols**

RTE = radiative transfer equation

MC = Monte Carlo

iMC = individual-photon tracking Monte Carlo

$R_d$  = diffuse reflectance

$T_d$  = diffuse transmittance

$T_c$  = collimated transmittance

$n_r$  = real refractive index

$\mu_a$  = absorption coefficient

$\mu_s$  = scattering coefficient

$g$  = anisotropy factor

$a$  = single-scattering albedo =  $\mu_s/\mu_t$

$L_a$  = total pathlength before absorption

$L_s$  = free pathlength between two consecutive scattering events

## Chapter 1 Inverse problems and radiative transfer

### §1.1 The inverse problem

Many scientific problems are expressed in the form of probing an unknown system by investigating its response to an excitation. If one can determine the excitation field and system's response through experimental measurements, these problems are then defined as the one to find a set of parameters for characterization of the system. In other problems, what are known and what are unknown may differ. Therefore, one tends to separate all parameters into three sets: the excitation field parameters, the response parameters and the system parameters. And all problems could be defined as finding one or more set(s) of parameter given the others. Normally, we define the forward problems as those to find the response parameters given the excitation and system parameters while the inverse problems as those to find the system parameters given the excitation and response parameters. How to define parameters? This would require a clear understanding of mechanism underlying a specific problem and the human's ability to relate it to observations or the measurables. For example, it would require a quantum mechanics based model to define the parameters such as absorption cross sections for characterization of atomic ability to absorb incident light.

For describing the response of a turbid sample of dimensions of 0.1mm or larger to the visible or near-infrared light, a radiative transfer theory, instead of classical electrodynamics, would be sufficiently accurate and manageable for obtaining analytical or numerical solutions. A radiative transfer equation (RTE) based on the energy conservation law can be used to describe the steady-state process of optical energy transportation inside a homogeneous turbid medium as (van de Hulst, 1980)

$$\mathbf{s} \cdot \nabla L(\mathbf{r}, \mathbf{s}) = -\mu_t L(\mathbf{r}, \mathbf{s}) + \mu_s \int_0^\pi \int_0^{2\pi} p(\mathbf{s}, \mathbf{s}') L(\mathbf{r}, \mathbf{s}') \sin \theta' d\theta' d\phi', \quad (1)$$

where  $L(\mathbf{r}, \mathbf{s})$  is the light radiance,  $\mathbf{r} = x\mathbf{x} + y\mathbf{y} + z\mathbf{z}$  with  $(\mathbf{x}, \mathbf{y}, \mathbf{z})$  as the unit vectors of respective Cartesian coordinate axis,  $\mathbf{s} = \sin\theta\cos\phi\mathbf{x} + \sin\theta\sin\phi\mathbf{y} + \cos\theta\mathbf{z}$  is the unit vector along the propagation direction of light and  $\mu_t = \mu_a + \mu_s$  is the attenuation coefficient.

The RTE, however, has to be supplemented by proper boundary conditions to form a well-posed boundary value problem for modeling of a specific system. A reasonable one appears to be given by the Fresnel formulae for plane electromagnetic waves (Born and Wolf, 1999) in which light transportation at an interface depends on the mismatch of the refractive index between the two neighboring media. Even though no analytical model exists for complex turbid media such as the human skin, experimental data on coherence reflectance curves demonstrate good agreement with the Fresnel formulae (Ding, 2005). Consequently, it became customary to use  $\mu_a$ ,  $\mu_s$ ,  $p(\mathbf{s}, \mathbf{s}')$  and the real refractive index  $n_r$  as the system parameters of a turbid medium.

Furthermore, the Henyey-Greenstein (HG) function  $p(\cos\theta)$  (Henyey and Greenstein, 1941; van de Hulst, 1980), where  $\cos\theta = \mathbf{s} \cdot \mathbf{s}'$ , has been widely used to represent phase functions in different turbid materials or at least as the window-smoothed ones. The HG function is a single-parameter function determined by the mean value of  $\cos\theta$ , i.e.,  $g = \langle \cos\theta \rangle$ , where  $g$  is called the anisotropy factor. With  $p(\cos\theta)$  as the phase function, optical

characterization of a turbid sample is thus reduced to the determination of 4 system parameters:  $(\mu_a, \mu_s, g, n_r)$ .

Base on the radiative transfer theory, the inverse problem described in this manual can then be summarized as the following: determine the system parameters  $(\mu_a, \mu_s, g, n_r)$  for a homogeneous turbid sample by measuring its response to a light beam of known wavelength and (absolute or relative) intensity. The refractive index  $n_r$  can be determined from the angular dependence of coherent reflectance without the need of an integrating sphere and has been described in details in (Ding, 2005). We therefore concentrate in this manual on the method for determination of  $(\mu_a, \mu_s, g)$  with an integrating sphere given the value of  $n_r$ .

## §1.2 The tools

When a light beam is incident on a turbid sample, the response is dominated by the absorption and elastic scattering within its volume. This causes the distribution of scattered light in many directions from the sample. Three optical configurations have been developed to solve the above inverse problem.

An integrating sphere is used to collect the light or photons in nearly all directions and re-distribute them uniformly over the inner surface of the sphere, which is of high reflectivity and surface roughness. A light detector is inserted into the detector port of the sphere to detect a small portion of the integrated light irradiance, which is proportional to the area ratio of the total inner surface of the sphere to that of the detector. The diffuse reflectance  $R_d$  and diffuse transmittance  $T_d$  can be measured with the sphere.

A spatial filtering setup is used to measure the relation between the light signal of collimated transmission  $I_f$  and sample thickness  $D$ . This relation allows estimation of the attenuation coefficient  $\mu_t$ .

A Monte Carlo (MC) method is used to obtain calculated diffuse reflectance  $R_{dc}$  and  $T_{dc}$  based on the framework of RTE and Fresnel formulae by simulating the photon transportation inside the sample and sample holder using the exact geometry and system parameters.

An inverse algorithm based on a gradient scheme is devised to determine the “true” values of scattering albedo  $a = \mu_s/(\mu_a + \mu_s)$  and  $g$  through iterations until a squared error function

$$\delta = \left( \frac{R_d - R_{dc}}{R_d} \right)^2 + \left( \frac{T_d - T_{dc}}{T_d} \right)^2, \quad (2)$$

is reduced to a threshold, i.e.,  $\delta < \delta_m$ , where  $\delta_m = 4 \times 10^{-4}$  is a typical value consistent with the total experimental errors in the  $R_d$  and  $T_d$  measurements.

In addition, we also build a MC based code to simulate the photon transportation between an integrating sphere and sample/sample holder to validate some of the equations we used to relate the measured and calculated  $R_d$  and  $T_d$  (Chen, 2006). In this code, we simulate light absorption and scattering in a turbid sample by tracking individual photons instead of photon packets as other types of MC codes (Wang, 1995).

## Chapter 2 Signal measurement

### §2.1 Measurement of light signals of collimated transmission

The measured signals of collimated transmitted light signal  $I_f$  as a function of a slab sample of thickness  $D$  can be used to estimate the attenuation coefficient from the following relation (the Beer-Lambert law):

$$I_f(D) \approx SI_0 e^{-\mu_t D} \quad (3)$$

where  $S$  is a numerical factor representing surface effect such as reflection loss. For samples of strong attenuation, with  $\tau = \mu_t D > 4$ , the measured  $I_f$ - $D$  data deviates significantly from a straight line on a semi-log plot. In these cases, the estimated  $\mu_t$  values were determined mainly by the two data points of the smallest  $D$  values because these  $I_f$  values are much larger than others at large  $D$  values and their statistical weights dominate others in the least-squares fitting. Two cases of  $I_f(D)$  are shown in Fig. 1 (Chen, 2006). The values of  $\mu_t$  and  $n_r$  are then used as the input parameters for inverse determination of the albedo  $a = \mu_s/\mu_t$  and anisotropy factor  $g$  from the measured signals of  $R_d$  and  $T_d$ .

Because of the weak irradiance from a non-coherent light source and large optical thickness  $\tau = \mu_t D$ , the measured data of  $I_f(D)$  over a large range of  $D$  may require detection of very weak signals.

This could be further complicated if a photodiode, rather than a photomultiplier, has to be used as detector for large spectral region of sufficient sensitivity and compactness. Therefore, a preamplifier with very high impedance gain may be needed to convert the current signals of the photodiode into a voltage signal for lock-in detection. In our measurements, we used a preamplifier with gains as high as  $10^{11}(\Omega)$  combined with a lock-in amplifier of long integration time (up to 30s) to obtain acceptable signal-to-noise ratios. The modulation frequency of the incident light is set to 17Hz for the narrow bandwidth preamplifier.

### §2.2 Measurement of diffuse reflectance and transmittance

The measured data of  $R_d$  and  $T_d$  of relatively high signal-to-noise ratios are obtained with an integrating sphere for its insensitivity to sample and detector alignment. The principle of the integrating sphere has been discussed by many authors (Goebel, 1967; Pickering, 1993). In particular, the configuration of the integrating sphere and equations concerned in this

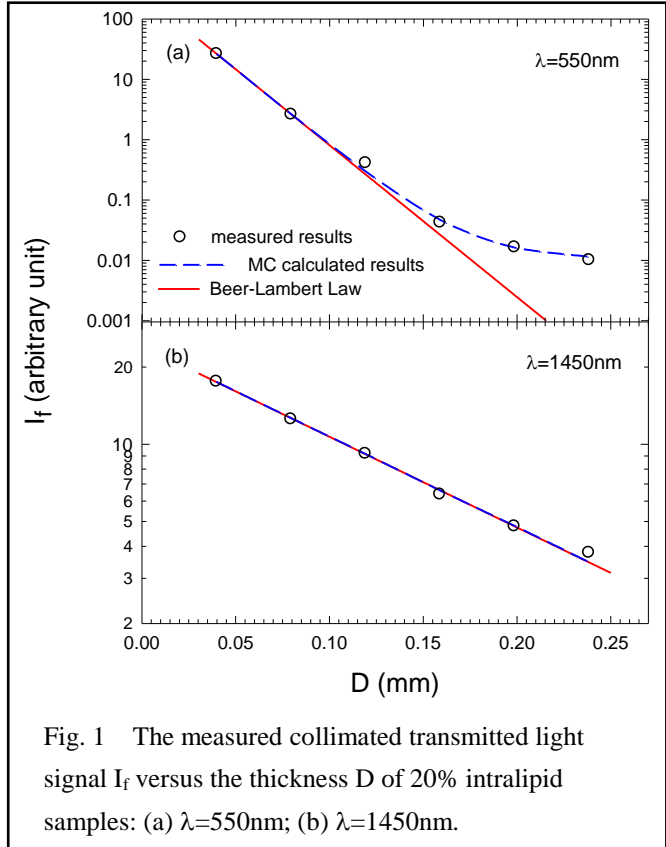


Fig. 1 The measured collimated transmitted light signal  $I_f$  versus the thickness  $D$  of 20% intralipid samples: (a)  $\lambda=550\text{nm}$ ; (b)  $\lambda=1450\text{nm}$ .

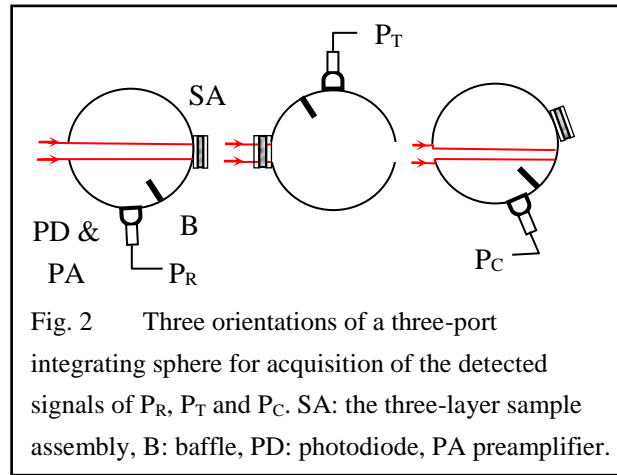
manual have been described in details in (Du, 2000). The sample assembly is installed on one of the three ports of an integrating sphere, and the other two ports are used for incident/exit light beam and detector. We measure three signals, ( $P_R$ ,  $P_T$ ,  $P_C$ ), by placing the sphere in three orientations as shown in Fig. 2. The experimental data of  $R_d$  and  $T_d$  are then obtained through the following equations (Du, 2000)

$$R_d = \frac{AP_R \cos 20^\circ}{A(1-f)P_C + A_s P_R \cos 20^\circ}, \quad (4)$$

$$T_d = R_d \frac{P_T}{P_R}, \quad (5)$$

where  $A=4\pi R^2$  is the total surface area of the sphere,  $f$  is the area ratio of the three ports in the sphere to  $A$  and  $A_s$  is the circular area of the sample assembly exposed to the integrating sphere. The factor of  $\cos 20^\circ$  in Eq. (4) is used to account for the decreased power into the sphere for the  $P_C$  measurement at the oblique orientation of  $20^\circ$  from the  $P_R$  measurement if the incident beam illuminates fully the entrance aperture of the sphere.

It should be pointed out here that the Eqs. (4) and (5) are derived under the assumption of a single sample with diffuse reflectance  $R_d$  and transmittance  $T_d$  (Du, 2000). In reality, liquid or soft tissue samples have to be placed in a glass holder to form a three-layer sample assembly for these measurements. Furthermore, one observes that the light or photons are “bounced” between the sphere and the sample assembly many times before they are either absorbed, by the sample or the detector or the sphere, or excluded from the system by escaping into the free space. These “optical facts” are quite different from the ideal configuration of photon counting assumed in the MC simulations (see Fig. 3 and §3.2). Therefore, these discrepancies need to be examined carefully to assure the accuracy of experimental measurements and theoretical modeling. We investigated the effects of these discrepancies with a sphere MC code to track photons exactly as they transport between the sample assembly and sphere. Comparison of the  $R_{dc}$  and  $T_{dc}$  calculated from these two MC codes shown that Eqs. (4) and (5) are sufficiently accurate in deriving the measured values of  $R_d$  in comparison with calibrated diffuse reflectance standards (Chen, 2006).



## Chapter 3 The Monte Carlo code

### §3.1 Essence of Monte Carlo (MC) simulation

MC simulation is a statistical method that can be used to solve the boundary value problems with or without stochastic nature. In this method, a physical problem involving interaction between an excitation field and a system described by the integral/differential equations and boundary conditions is simulated by random processes conforming to a set of statistical rules. These rules must be designed so that the physical principle underlying the interaction can be realized in the simulations. The response of the system can then be expressed in terms of the mean values of the simulated quantities with a variance inversely related to the number of simulated particles. Obviously, accurate results of MC methods are only possible by performing a large number of simulations. MC method has a long history of application in modeling coupled transport of electrons and neutral particles (neutrons and photons) in condensed matters and a version of the simulation codes have been in public domain since 1985 (Nelson, 1985). Much of the algorithms employed in the existing MC codes for modeling light-tissue interaction (Prahl, 1989; Wang, 1995; Song, 1999) can be traced backed to these early works.

For a boundary problem consisting of RTE equation, Eq. (1), and Fresnel formulae, MC simulations can be performed by tracking the transportation of  $N$  independent particles of photons in a sample system characterized by a given set of optical parameters ( $\mu_a$ ,  $\mu_s$ ,  $g$ ), if the HG phase function  $p(\cos\theta)$  is assumed. Appropriate statistical distributions for the pathlengths and scattering angles should be applied to track the photons interacting with the turbid medium characterized by the above optical parameters. The trajectories of  $N$  photons undergoing scattering and absorption events are simulated individually and tallied at the end of simulations to obtain a system response in terms of diffuse reflectance  $R_d$ , diffuse transmittance  $T_d$  and light signals of collimated transmission  $I_f$  that are experimentally observable.

MC simulation has a long history of use in calculating particle transportation. The first attempt to use MC simulation for calculation of light distributions was reported by Wilson et al. (Wilson and Adam, 1983). This effort has been followed with a significantly improved algorithm by several other researchers (Keijzer, 1989; Prahl, 1989; Wang, 1995). Based on these works, we have proposed a slightly different algorithm termed as individual photon tracking monte Carlo or iMC with improved simulation speed and ease of implementation with high performance computation techniques (Song, 1999). The iMC code used for generating the calculate data for comparison with the measured data has been built with this algorithm on the basis of earlier versions (Dong, 1999; Du, 2001; Ma, 2003; Ma, 2003; Ma, 2005). In addition, we utilized the structural design of a published MC code of photon tracking in a multi-layer slab sample by Wang and Jacques (Wang, 1995) to improve our algorithm for a streamlined code design on photon tracking. We briefly describe the major features of the iMC code in this section, followed by the code details and the inverse determination of optical parameters in the next two sections.

To simulate light transportation through a three-layer sample assembly,  $N$  photons are injected into the assembly in a direction perpendicular to the sample surface and their 3D trajectories are followed inside the sample assembly until they exit. The scattering and absorption of a tracked photon are simulated as random events with probability distribution

functions dictated by scattering and absorption coefficients, respectively. The probability distribution function for a free pathlength  $L_s$  of the tracked photon between two scattering events is assumed as (Prahl, 1989)

$$P(L_s) = \mu_s e^{-\mu_s L_s}. \quad (6)$$

The parameter  $L_s$  is sampled from a uniformly distributed random numbers (RND) between 0 and 1 through the following transformation to satisfy Eq. (6)

$$L_s = -\ln(1 - RND) / \mu_s = -\ln(RND) / \mu_s. \quad (7)$$

Similarly, the total pathlength of a photon traveled before being absorbed in the sample,  $L_a$ , is obtained from

$$L_a = -\ln(1 - RND) / \mu_a = -\ln(RND) / \mu_a. \quad (8)$$

Before a photon is injected at the sample-glass interface, its total pathlength  $L_a$  is first determined from Eq.(8). Then the parameter  $L_s$  is determined from Eq.(7) each time before the tracked photon is allowed to travel before next scattering. Using the HG function  $p(\cos\alpha)$  as the single-scattering phase function, the distribution functions of the azimuthal ( $0 \leq \phi \leq 2\pi$ ) and polar scattering angles ( $0 \leq \alpha \leq \pi$ ) for a scattered photon are given by

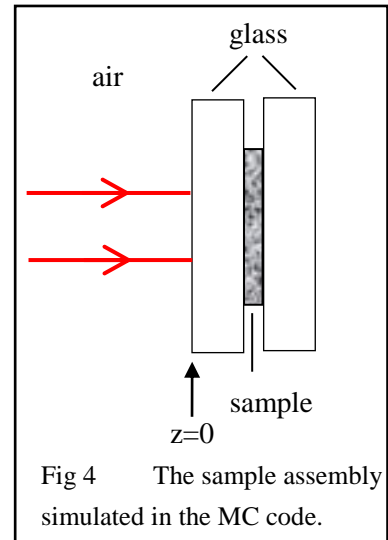
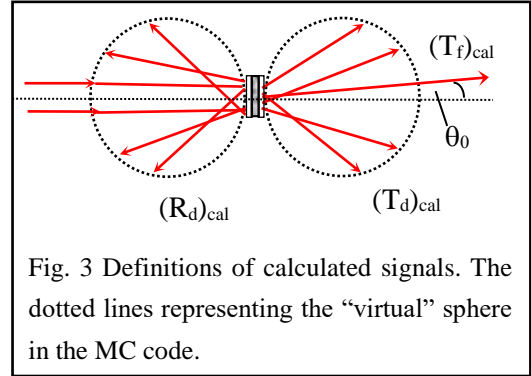
$$P(\cos \alpha) = \frac{(1-g^2)}{2(1+g^2-2g \cos \alpha)^{3/2}}, \quad (9)$$

$$P(\phi) = \frac{1}{2\pi}. \quad (10)$$

Once the tracked photon exit from the three-layer sample assembly, the position and the direction of the photon at the exit surface will be used to determine if the photon contributes to a signal that can be measured, as shown by Fig. 3. After the tracking of  $N$  injected photons, the number of the outgoing photons are tallied to obtain the calculated data of  $(R_d)_{cal} = N_{R_d}/N$ ; diffuse transmittance  $(T_d)_{cal} = N_{T_d}/N$ , and collimated (unscattered) transmittance  $T_c$ .

### §3.2 Details of iMC code

The iMC code has been developed in Fortran 90 to simulate photon transportation inside and outside of a three-layer sample assembly in air, as show in Fig. 4, according to the experimental configuration used in the sphere measurement. A turbid slab sample is held between two glass plates in which the light scattering and absorption are negligible. There are four parallel interfaces: 2 tissue-glass interfaces and 2 glass-air interfaces. Photon refraction and reflection at these interfaces are considered based on the Fresnel formulae to satisfy the boundary value problem described in Chapter 1.



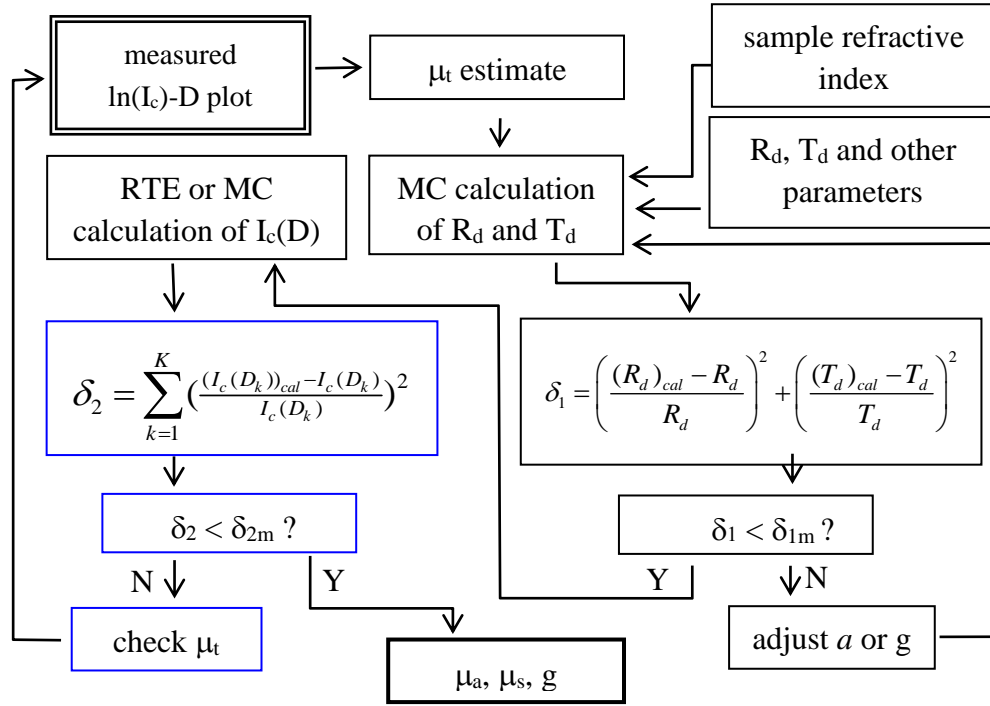


Fig. 5 The flowchart of the iMC code. The functions of the blocks with blue lines are not included in the software.

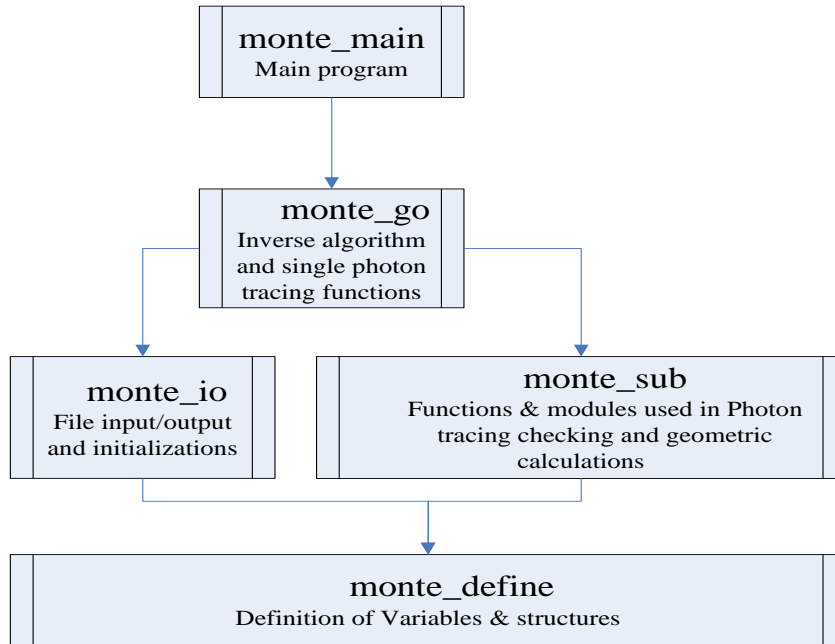


Fig. 6 The iMC code structure.

At start, the iMC code gathers the attenuation coefficient  $\mu_t$ , refractive indices of the sample and glass plates, measured  $R_d$  and  $T_d$  and other geometric parameters as the input parameters. After tracking of  $N$  injected photons, the iMC code employs a gradient-based searching algorithm to find the optical parameters  $a$  and  $g$  of the turbid sample that produce calculated values of  $R_d$  and  $T_d$  matching the measured ones within the experimental errors.

This is achieved by minimizing the squared error function given in Eq. (2) iteratively until  $\delta < \delta_m$  is satisfied.

The iMC code consists of a main program (`monte_main`) with four major modules: `monte_define`; `monte_io`; `monte_sub` and `monte_go`. Figs. 5 and 6 illustrate a flow chart and the code structure of the software.

### §3.2.1 *monte\_define*

This module declares a collection of input data in the forms of derived data types used by other modules: input parameters of I/O file names, experimental parameters and  $R_d$  and  $T_d$  (INPUTSTRUCT); photon coordinates and other tracking variables which are updated each time a new photon is injected (PhotonStruct); layer optical ( $\mu_a$ ,  $\mu_s$ ,  $g$ ,  $n$ ) and geometrical parameters (LayerStruct); output data and simulation parameters (OutputStruct). For more details please read the comments included in the code. Constants are predefined number such as  $\pi$ , seeds for the random number generator, etc..

### §3.2.2 *monte\_io*

This subroutine contain all the functions and subroutines which are used to read and write the files, print result on the screen and initialize the program.

### §3.2.3 *monte\_sub*

This module deals with photon injection, photon-interface interaction based on the Fresnel formulae, random number generation, photon tracking and other subroutine to handle geometric calculations. Details about the functions of each module are given by the notes and comments in the code.

### §3.2.4 *monte\_go*

This module contains the subroutines to simulate the photon-sample interaction by tracking one photon transporting in and out of the sample assembly with various interfaces and to inversely calculate the optical parameters ( $\mu_a$ ,  $\mu_s$ ,  $g$ ) by matching the calculated  $R_d$  and  $T_d$  with the measured ones. The structure of this module is mainly based on the C code developed by Wang and Jacques (Wang, 1995) and a flow chart is presented in Fig. 7.

With a Cartesian coordinate system ( $x$ ,  $y$ ,  $z$ ), a turbid sample of thickness  $z_0 = D$  is placed between two glass plates with the photons injected at the glass-sample interface on the glass side:  $z = 0^-$ . The photons in the incident beam are injected at the first air-glass interface with a meshed circle of area  $\pi r^2$ , where the parameter  $r$  is the radius of the collimated incident beam and a control number  $NR0$ , defined as  $NR0 = \sqrt{N / \pi}$ , is used in the code to mark the total injected photon number. The subroutine "beam" provides the coordinates of each grid cell in the mesh.

After injection, the photon is tracked by following a series of scattering events until it becomes absorbed or exits from the tracking region. The total pathlength  $L_a$  traversed by a photon before being absorbed is selected randomly from a distribution described by Eq. (8) (see SUBROUTINE LaunchPhoton). Similarly, the distance  $L_s$  between two consecutive scattering events is selected according to Eq. (7) (see SUBROUTINE StepSizeInTissue). The scattering angles are obtained by Eq. (9) and (10) using the SUBROUTINE Spin. At each scattering event,  $L_a$  is reduced by the updated  $L_s$  and is checked to see if it becomes negative.

If no, the tracking continues. Otherwise the tracking stops and the photon is assumed to be absorbed.

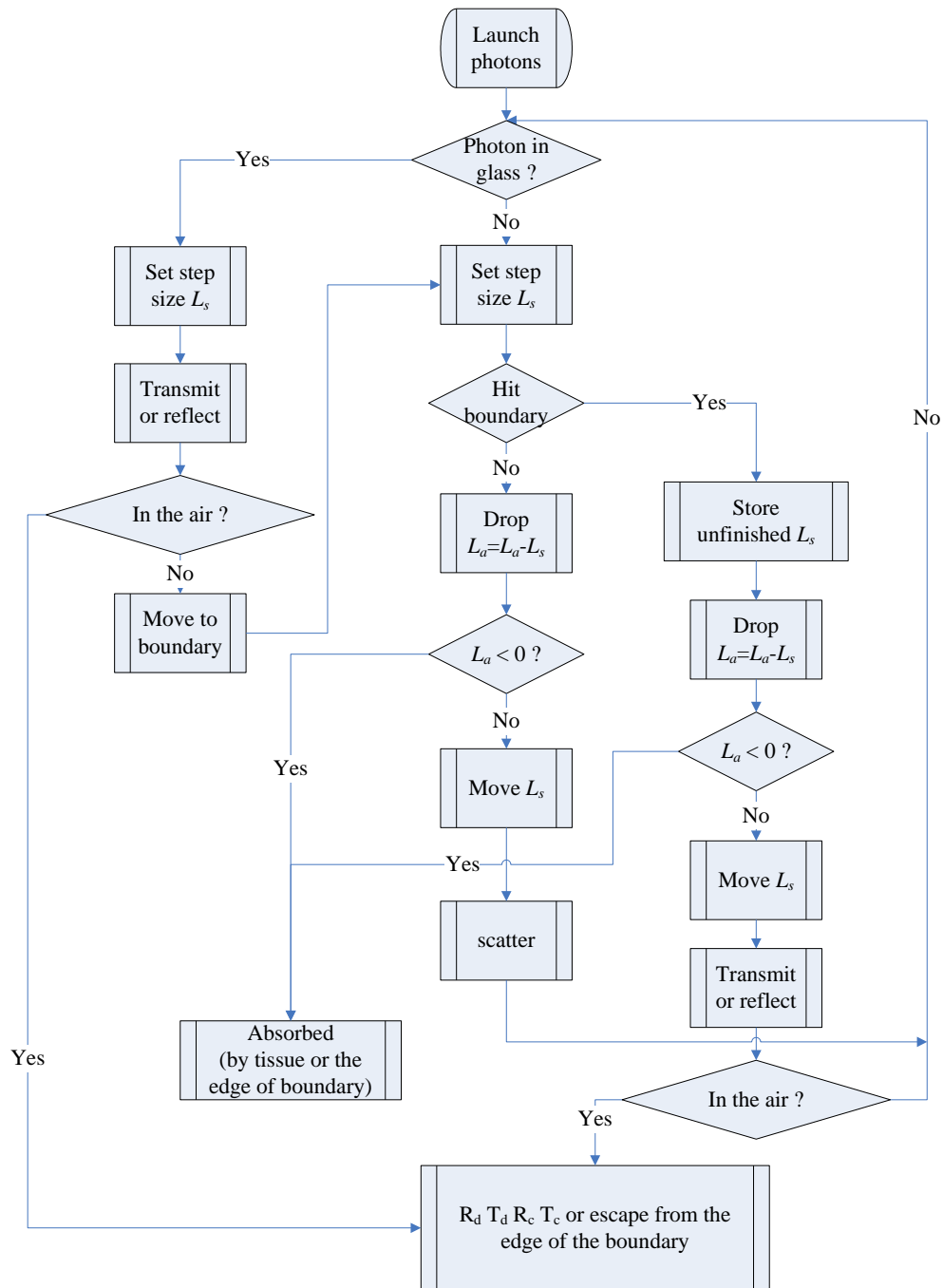


Fig. 7 The flow chart of iMC code for tracking a photon in the sample assembly.

§3.2.5 monte\_main

This module is the main program to call other modules. The main program first calls the subroutine "initialize" to read the optical and geometrical parameters of the sample assembly and measured data set from the file "file-c" and then execute the inverse calculation for each

set of measured data at a given wavelength unit all optical parameters of the sample are determined in the desired spectral region.

### §3.3 How to run the iMC code?

The iMC code package includes three files in addition to the five modules described in the last section: (1) a file (*makefile*) to be used together with the five modules to generate an executable file of "*monte\_main*"; (2) a file (*file-c*) containing constant input parameters to be read by the main module; (3) a file (*file-v*) containing variable input parameters such as refractive indices of glass and sample, measured  $R_d$  and  $T_d$ , which are dispersive. The output of the code is written into a file with the name of "file-out". A user needs to copy all five modules and the file of "makefile" into one directory at a host computer with UNIX/LINUX operating system and type "make" to start execution.

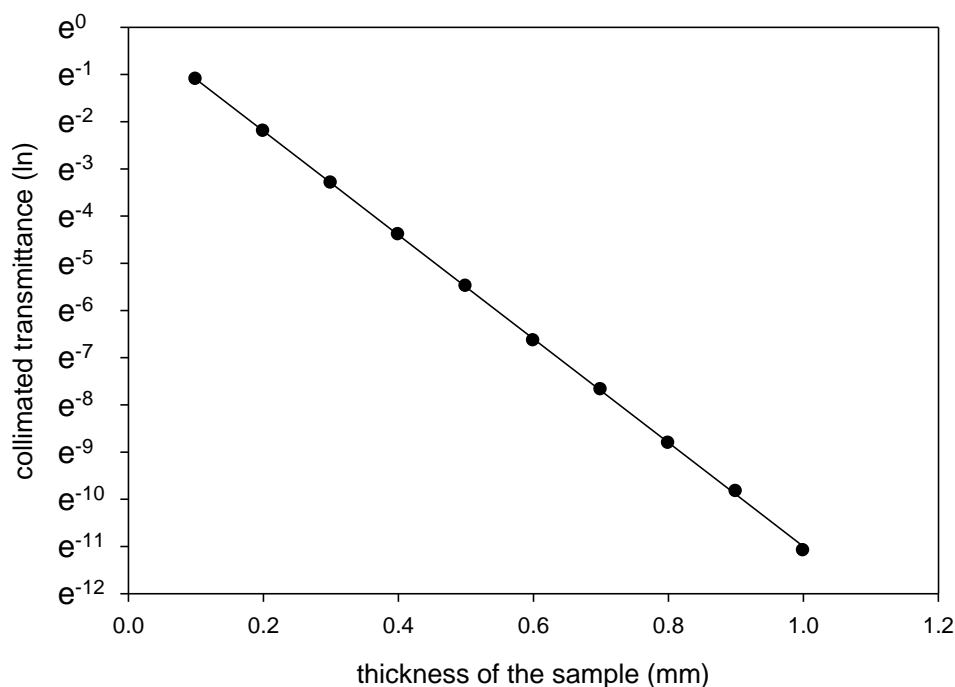


Fig. 8 Comparison of MC calculated collimated transmittance (symbols) with those from the Beer-Lambert law (solid line).

### §3.4 Code validation

We compare the collimated transmittance  $T_c$  calculated by the iMC code, as the number ratio of unscattered and transmitted photons to the incident photon, to the calculated values based on the Beer-Lambert Law (see Eq. (3) with  $T_c = SI_f/I_0$ ). In the data presented in Fig. 8, the following parameters are adopted: a single sample of infinite size in the x-y plane without glass plates and with  $\mu_a = 1.000 \text{ mm}^{-1}$ ,  $\mu_s = 10.0 \text{ mm}^{-1}$ ,  $g = 0.500$ ,  $n = 1.000$ . Additional validations of the MC code can be made by comparing the MC calculated signals of  $I_f$  to the RTE solution in (Chen, 2006).

Validation of the iMC code for photon tracking in a single-layer sample is also carried out by comparing the angle-resolved bidirectional reflection and transmission functions R and T with the RTE solutions from the Table 35 of (van de Hulst, 1980), and the result are show in Fig. 9.

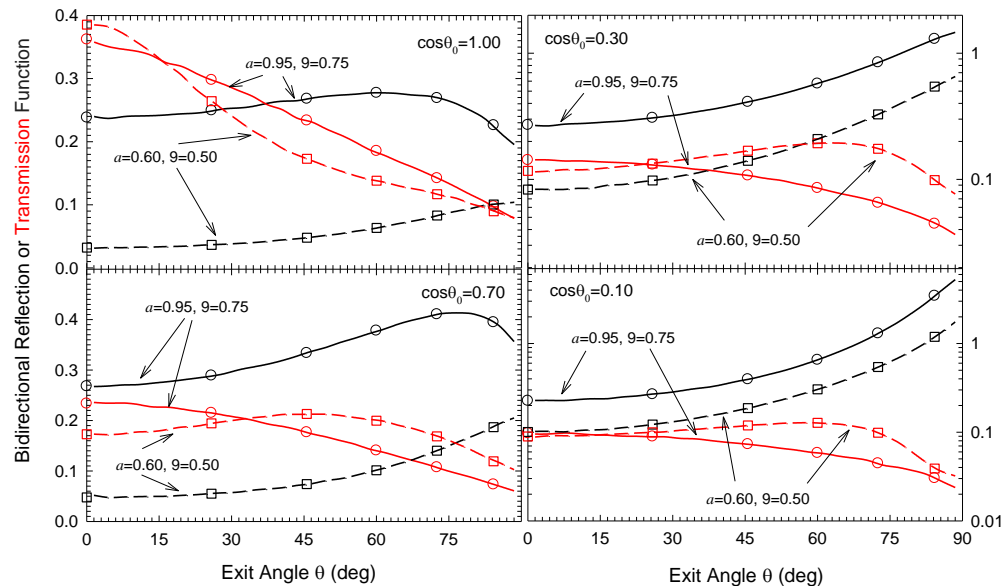


Fig. 9 The bidirectional reflection and transmission functions versus the exit angle  $\theta$  for a homogeneous slab phantom of  $n_r=1.00$  with  $N=1.26 \times 10^7$ . Two groups of phantom parameters were used: (1)  $a=0.95$  ( $\mu_a=0.50\text{mm}^{-1}$ ,  $\mu_s=9.50\text{mm}^{-1}$ ),  $g=0.75$ ,  $D=0.80\text{mm}$ ; (2)  $a=0.60$  ( $\mu_a=4.00\text{mm}^{-1}$ ,  $\mu_s=6.00\text{mm}^{-1}$ );  $g=0.50$ ;  $D=0.10\text{mm}$ . The black (red) lines are the bidirectional reflection (transmission) functions calculated by the iMC code while the black (red) symbols are the corresponding values from the Table 35 of (van de Hulst, 1980) with  $\theta_0$  as the incident angle.

## References

- Born, M. and E. Wolf (1999). Principles of Optics. Cambridge, England, Cambridge University Press.
- Chen, C., J. Q. Lu, et al. (2006). "A primary method for determination of optical parameters of turbid samples and application to intralipid between 550 and 1630nm." Opt. Express **14**(16): 7420-7435.
- Ding, H., J. Q. Lu, et al. (2005). "Determination of refractive indices of porcine skin tissues and intralipid at eight wavelengths between 325 and 1557nm." J. Opt. Soc. Am. A **22**: 1151-1157.
- Dong, K. (1999). Monte Carlo Simulation of Converging Laser Beams Propagating in the Skin Tissue Phantoms with Random Rough Surfaces MS Thesis, East Carolina University.
- Du, Y. (2000). Optical Properties of Porcine Dermis in the Near Infrared Region between 900nm and 1500nm MS, East Carolina University.

- Du, Y., X. H. Hu, et al. (2001). "Optical properties of porcine skin dermis between 900 nm and 1500 nm." Phys. Med. Biol. **46**(1): 167-181.
- Goebel, D. G. (1967). "Generalized integrating-sphere theory." Appl. Opt. **6**: 125-128.
- Heney, L. G. and J. L. Greenstein (1941). "Diffuse radiation in the galaxy." Astrophys J **93**: 70-83.
- Keijzer, M., S. L. Jacques, et al. (1989). "Light distributions in artery tissue: Monte Carlo simulations for finite-diameter laser beams." Lasers Surg Med **9**(2): 148-154.
- Lu, J. Q., X. H. Hu, et al. (2000). "Modeling of the rough-interface effect on a converging light beam propagating in a skin tissue phantom." Appl. Opt. **39**(31): 5890-5897.
- Ma, X., J. Q. Lu, et al. (2003). "Determination of Complex Refractive Index of Polystyrene Microspheres from 370 to 1610nm." Phys. Med. Biol. **48**(24): 4165-4172.
- Ma, X., J. Q. Lu, et al. (2005). "Bulk optical parameters of porcine skin dermis tissues at eight wavelengths from 325 to 1557nm." Opt. Lett. **30**(4): 412-414.
- Ma, X., J. Q. Lu, et al. (2003). "Effect of surface roughness on determination of bulk tissue optical parameters." Opt. Lett. **28**(22): 2204-2206.
- Nelson, W. R., H. Hirayama, et al. (1985). "The EGS4 Code System." from <http://www.slac.stanford.edu/pubs/slacreports/slac-r-265.html>.
- Pickering, J. W., S. A. Prahl, et al. (1993). "Double-Integrating-Sphere System for Measuring the Optical-Properties of Tissue." Appl. Opt. **32**(4): 399-410.
- Prahl, S. A., M. Keijzer, et al. (1989). A Monte Carlo Model of Light Propagation in Tissue. SPIE Institute Series, SPIE Proceeding.
- Song, Z., K. Dong, et al. (1999). "Monte Carlo simulation of converging laser beams propagating in biological materials." Appl. Opt. **38**(13): 2944-2949.
- van de Hulst, H. C. (1980). Multiple light scattering: tables, formulas, and applications. New York, Academic Press.
- Wang, L., S. L. Jacques, et al. (1995). "MCML--Monte Carlo modeling of light transport in multi-layered tissues." Comput Methods Programs Biomed **47**(2): 131-146.
- Wang, L., S. L. Jacques, et al. (1995). "MCML-Monte Carlo modeling of light transport in multi-layered tissues." Comput. Meth. Prog. Bio. **47**(2): 131-146.
- Wilson, B. C. and G. Adam (1983). "A Monte Carlo model for the absorption and flux distributions of light in tissue." Med Phys **10**(6): 824-830.